Taylor & Francis
Taylor & Francis Group

Inhalation Toxicology

International Forum for Respiratory Research

ISSN: 0895-8378 (Print) 1091-7691 (Online) Journal homepage: http://www.tandfonline.com/loi/iiht20

Numerical Simulations Investigating the Regional and Overall Deposition Efficiency of the Human Nasal Cavity

Kevin T. Shanley, Parsa Zamankhan, Goodarz Ahmadi, Philip K. Hopke & Yung-Sung Cheng

To cite this article: Kevin T. Shanley, Parsa Zamankhan, Goodarz Ahmadi, Philip K. Hopke & Yung-Sung Cheng (2008) Numerical Simulations Investigating the Regional and Overall Deposition Efficiency of the Human Nasal Cavity, Inhalation Toxicology, 20:12, 1093-1100, DOI: 10.1080/08958370802130379

To link to this article: https://doi.org/10.1080/08958370802130379

Inhalation Toxicology, 20:1093–1100, 2008

ISSN: 0895-8378 print / 1091-7691 online
DOI: 10.1080/08958370802130379

informa
healthcare

Numerical Simulations Investigating the Regional and Overall Deposition Efficiency of the Human Nasal Cavity

Kevin T. Shanley, Parsa Zamankhan, and Goodarz Ahmadi
Department of Mechanical and Aeronautical Engineering Clarkson University, Potsdam, New York

Philip K. Hopke
Department of Chemical and Biomolecular Engineering, Clarkson University, Potsdam, New York

Yung-Sung Cheng
Lovelace Respiratory Research Laboratory, Albuquerque, New Mexico, USA

Numerical simulations have been carried out on a model of the right passageway of an anonymous, adult male's nasal cavity, constructed from magnetic resonance imagery (MRI) scans. Steady, laminar, inspiratory flow was assumed to simulate inhalation. Analysis shows smoothly varying streamlines with a peak in velocity magnitude occurring in the nasal valves and a peak in vorticity magnitude immediately posterior. Dilute, uniform concentrations of inertial (1 μm $\leq d_{ae} \leq$ 10 μm) particles were released at the nostril and tracked via a Lagrangian tracking algorithm. Deposition efficiency is shown to increase with particle size and flow rate. Preferential deposition is seen in the anterior third of the nasal cavity for large Stokes number particles. An empirical expression for particle deposition is proposed that incorporates particle size, flow rate, and nose anatomy.

Due to the highly tortuous nature of the human nasal cavity, it is possible for different flow regimes (laminar, transitional, and turbulent) be represented within the passageway during normal breathings. The passageway of a human nasal cavity spans on the order of 10 cm. Its size and complexity make the computational modeling of air flow in the nasal passage quite challenging.

Historically, quantitative measurements of the airflow velocity field in the human nasal cavity have been difficult, due to the complexity and the small scale of the passages. In addition, the measuring instrumentation may significantly alter the flow field due to the small size of the airways, skewing the results. Nevertheless, a number of investigators have employed different techniques to collect meaningful data without significantly distorting the airflow.

Received 4 March 2008; accepted 15 April 2008.

The support of the National Institute for Occupational Safety and Health (NIOSH) through grant R01 OH003900 and the U.S. EPA under grant 916716 is gratefully acknowledged. This work has not been subjected to either agency's required peer or policy review and therefore does not necessarily reflect the views of the agencies and no official endorsement shall be inferred.

Address correspondence to Prof. Goodarz Ahmadi, Clarkson University, Department of Mechanical and Aeronautical Engineering, 8 Clarkson Avenue, Potsdam, NY 13699-5700, USA. E-mail: ahmadi@clarkson.edu

In their pioneering work, Swift and Proctor (1977) used a miniature Pitot tube in different locations within their life-sized nasal passage replica to take velocity measurements. Schreck et al. (1993) used CAD software to scale the magnetic resonance imagery (MRI) data 300%, from which a 3 times life size replica was fabricated. They took velocity measurements at different locations with a hot-wire anemometer. Another enlarged replica was made by Hahn et al. (1993). This replica was 20 times life size, and a hot-film anemometer was used to make localized velocity measurements.

Particle image velocimetry (PIV) has proven to be an important velocity measurement tool because of its noninvasive nature. The scale of the replicas can be brought back down to life size, and many investigators have noted its usefulness (e.g., Kelly et al., 2000; Churchill et al., 2004; Kim & Chung, 2004).

While the details vary slightly among different studies, they all share agreement in the general trend of the data. All measurements in the literature reported that the flow is laminar for low to moderate breathing rates ($\leq$25 L/min). Swift and Proctor (1977) and Schreck et al. (1993) reported observing vortices posterior to the nasal valves, while Kelly et al. (2000) observed the highest velocity magnitude at the location of the nasal valve. Both of these observations are in agreement with what would be expected of the basic fluid dynamic of the flow through passages of varying cross section. Qualitatively, all studies agree that the

majority of inspired air passes through the inferior portion of the cavity (inferior and middle meati), while significantly less flow passes through the superior regions, including the olfactory slit.

Keyhani et al. (1995) and Subramanian et al. (1998) employed a steady laminar flow model to simulate human inhalation. Both of these works used the commercially available finite-element method (FEM)-based software FIDAP (Fluent, Inc., Lebanon, NH). The qualitative observations of a majority passing through the inferior portion of the cavity were confirmed by these computational studies.

Shi et al. (2006) challenged the assumption that inhaled airflow was steady. Their work investigated steady inhalation, as well as the acceleration and deceleration phases of an idealized breathing cycle. They found under transient flow conditions nanoparticles deposited less frequently than under steady flow conditions with the same mean inlet velocity.

A comparison of turbulence models by Liu et al. (2007) shows a peak in turbulence intensity immediately posterior to the nasal valves, where vortices had been observed by Swift and Proctor (1977) and Schreck et al. (1993). Their work also shows a sharp decline in turbulence intensity with distance into the nasal cavity.

Particulate matter (PM) may be introduced into the environment by natural or human means. Natural phenomena such as volcanoes and forest fires account for a majority of the PM found in our atmosphere. While anthropogenic PM accounts for on the order of 10% of the total PM found in the environment, it is particularly of concern as it can be highly toxic and concentrated in microenvironments where humans spend most of their time (e.g., homes and work).

The inhalability of aerosols is a function of particle size and of PM concentration near the nostril. It is postulated that the body heat generates a thermal plume elevating the size of PM passively inhalable to 135 μm in calm air observed in some human subjects studied (Dai et al., 2006). The greatest risks to human health, however, are associated with PM_{10} (Pope, 2000; U.S. IPA, 1996).

A series of in vivo studies of PM deposition in human nose was performed by Thorsson et al. (1993), Newman et al. (1995), and Cheng et al. (1996). In addition, Cheng et al. (2001), Janssens et al. (2001), Kelly et al. (2004), and Su and Cheng (2005) report a number of in vitro studies of transport and deposition of particles in the nasal cavity. Numerical experiments have been conducted to investigate the deposition of particles in human nasal cavities by Zamankhan et al. (2006) and Shi et al. (2007), among others. Fortunately, the results of in vitro studies on plastic and resin replicas compare favorably with similar studies done on human subjects (Martonen & Zhang 1992; Cheng et al., 2001; Zwartz & Guilmette, 2001). The numerical work agrees favorably as well and provides an additional level of flexibility not capable in a laboratory setting (Shi et al., 2007). These works indicate higher deposition with increasing particle size for inertial particles, with nearly 100% deposition for particles having diameter larger than 10 μm.

A detailed analysis of published in vivo and in vitro experiments by Cheng (2003) resulted in an empirical expression for deposition of inertial aerosols. Impaction deposition efficiency is expressed as a function of Stokes number.

This study is focused on the deposition of inertial (1 μm $\leq d_{ae} \leq$ 10 μm) particles in the human nasal cavity. A steady-state laminar flow model as suggested by Swift and Proctor (1977), Schreck et al. (1993), and Kelly et al. (2000) with uniform inlet velocity recommended by Keyhani et al. (1995) was used to simulate inspiratory breathing conditions. The commercially available software FLUENT^{TM} was chosen to carry out the simulations because of its ability to easily and accurately handle unstructured tetrahedral meshes representing complex geometries. The flow is shown to be laminar for breathing rates of 3 and 6 L/min, with a peak in vorticity appearing posterior to the nasal valves. Deposition is shown to be dominated by impaction and heavily preferential toward the anterior end of the cavity. particularly as particle diameter increases.

COMPUTATIONAL MODEL

Computational Domain

MRI scans of an anonymous, healthy, adult male human subject were used to form the flow volume representing the right nasal passage. The slice data with separation distance of 3 mm were loaded into the preprocessing software GAMBIT and key perimeter points were identified. These points were then used to construct surfaces in the stream wise direction, adjoining the slices into a three-dimensional (3D) volume (Zamankhan et al., 2006). Figure 1a shows a subset of the slices used in reconstruction. The final computational domain stretching from the tip of the nose to the entrance to the nasopharynx is shown in Figure 1b. The volume was filled with tetrahedral elements totaling 965,000 and corresponding to 250,000 computational nodes. Further grid refinement showed no noticeable gains in accuracy. Figure 1c shows a slice in the main airway region with the representative triangular mesh.

Governing Equations

Airflow simulations are carried out by numerically solving the conservation of momentum and mass equations. The steady-state version of the conservation equations for incompressible flow is

$$\rho \mathbf{u} \cdot \nabla \mathbf{u} = -\nabla p + \mu \nabla^2 \mathbf{u} + \rho \mathbf{g} \quad [1]$$

$$\nabla \cdot \mathbf{u} = 0 \quad [2]$$

Here $\mathbf{u}$ is the fluid velocity, ρ is the constant mass density of the fluid, μ is the dynamic viscosity, p is the pressure, and $\mathbf{g}$ is the gravitational acceleration.

The FLUENT code is a finite-volume-based code. Discretization of the conservation equations is performed with the upwind scheme to a second-order accuracy, pressure–velocity coupling is performed with the SIMPLE scheme, and derivatives are computed via the Green–Gaus nod-based method (*Fluent User's Manual*, 2007).

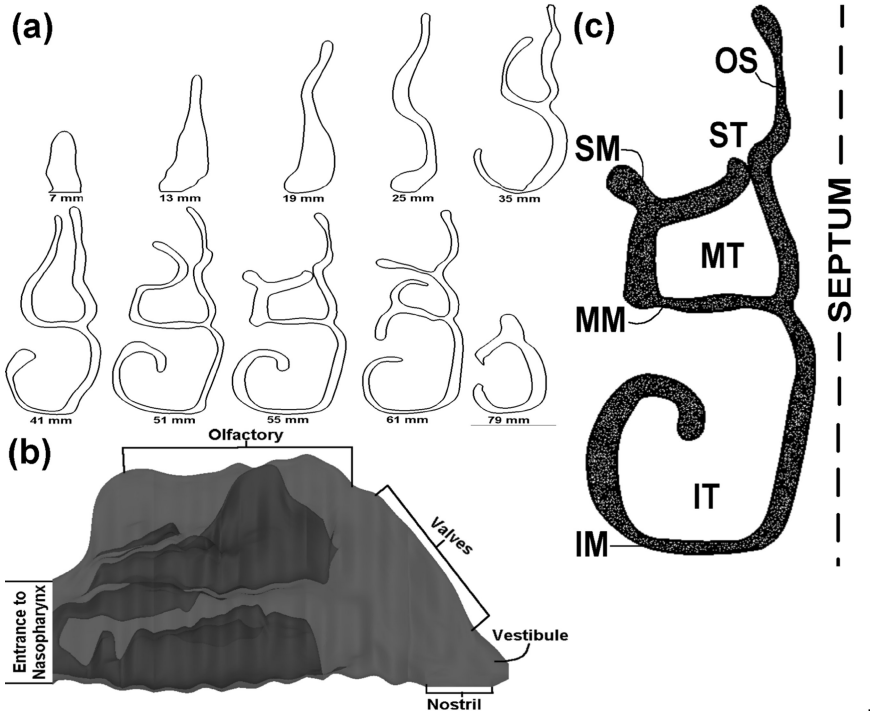

FIG. 1. (a) Subset of coronal cross sections used to construct the 3D volume, (b) 3D volume representing the right nasal passageway of an anonymous, adult, male, human subject stretching from the tip of the nose to the entrance of the nasopharynx, and (c) representative triangular faces on a coronal cross-section.

Boundary Conditions for Flow Analysis

The nostril and entrance to the nasopharynx were selected as the inlet and outlet surfaces of the computational domain, respectively. A uniform, constant-velocity profile was applied to the nostril inlet surface per the recommendations of Keyhani et al. (1995). Velocities corresponding to breathing rates of 2 to 7 L/min were simulated. The outlet surface was taken to be a planar surface posterior to the turbinates and anterior to the point at which both passages merge together in the nasopharynx. On this surface was applied the outflow boundary condition. Pressure and velocity values are an approximation on this surface. These approximations are made by extrapolating data from within the domain. The remaining surfaces were taken to be rigid, stationary, perfectly smooth walls with a no slip flow condition (*Fluent User's Manual*, 2007).

Lagrangian Particle Tracking

The discrete-phase model (DPM) within FLUENT is a Lagrangian particle tracking algorithm. Particle motion is governed by Newton's second law. That is,

$$\frac{du_i^p}{dt} = \frac{1}{\tau}\frac{C_{\mathrm{D}}\mathrm{Re}_p}{24}(u_i - u_i^p) + \frac{2\mathrm{K}\nu^{1/2}d_{ij}}{Sd(d_{lk}d_{kl})^{1/4}}(u_i - u_i^p) + g_i \quad [3]$$

In Eq. (3) $\mathbf{u}$ and $\mathbf{u}^p$ are the fluid and particle velocities, respectively, $\mathbf{g}$ is the gravitational acceleration, $\tau = C_C S d^2/(18\mu)$ is the particle relaxation time, S is the solid-to-gas density ratio, d is the particle diameter, μ is the fluid viscosity, $C_C = 1 + \frac{2\lambda}{d}\left[1.257 + 0.4e^{-1.1d/2\lambda}\right]$ is the Cunningham slip correction factor, λ is the mean free path of air, $\mathrm{K} = 2.594$ is the constant coefficient of Saffman lift force, $d_{ij} = \frac{1}{2}(\frac{\partial u_i}{\partial x_j} + \frac{\partial u_j}{\partial x_i})$ is the deformation rate tensor, $\mathrm{Re}_p = \frac{d|u_i - u_i^p|}{\nu}$ is the particle Reynolds number, and C_{D} is the drag coefficient given as (Hinds, 1982)

$$C_{\mathrm{D}} = \begin{cases} \frac{24}{\mathrm{Re}_p} & \text{for } \mathrm{Re}_p < 1 \\ \frac{24}{\mathrm{Re}_p}\left(1 + 0.15\mathrm{Re}_p^{0.687}\right) & \text{for } 1 < \mathrm{Re}_p < 400 \end{cases} \quad [4]$$

The terms on the right-hand-side of Eq. (3) represent the drag, lift, and gravitational forces per unit mass acting on the particle, respectively. Integration of Eq. (3) was performed with a backward Euler method. This method was selected for its stability independent of time step.

Boundary Conditions for Particle Tracking

A uniform concentration of particles was simulated at the nostril by releasing a single particle at the center of each computational cell on the inlet surface. The walls were assumed to be perfectly absorbing surfaces; that is once a particle came in contact with a wall it was considered trapped. Contact between walls and surfaces were assumed to occur once the distance between the center of mass of the particle and the wall

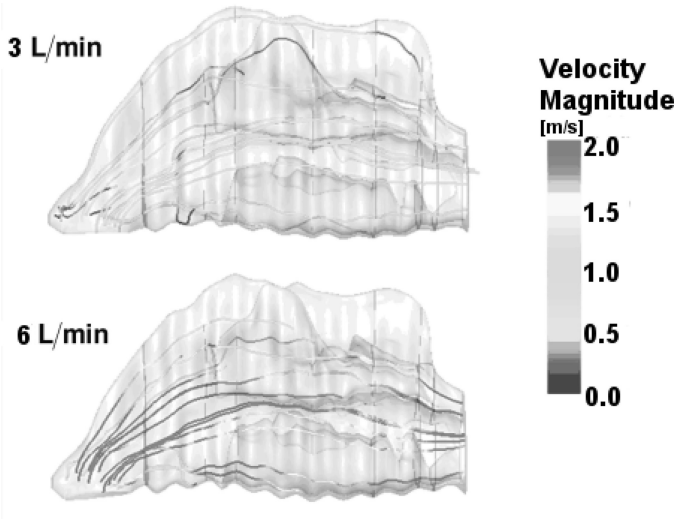

FIG. 2. Streamlines injected from several locations on the nostril surface for 12 L/min and 6 L/min volumetric flow rates.

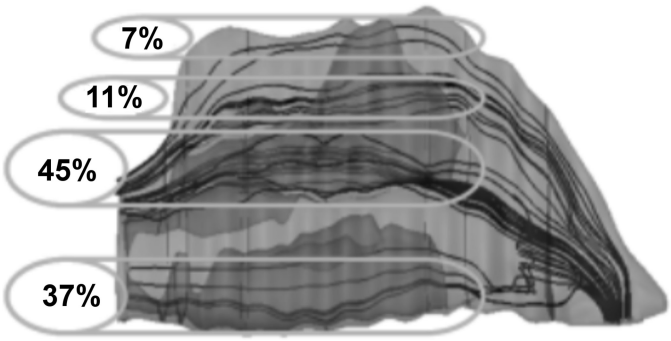

FIG. 4. Qualitative observations of regional volumetric flow.

became less or equal to the particle radius. Both the inlet and outlet allowed particles to pass through unperturbed without replacement.

RESULTS

Simulated Airflow

Simulations were performed to investigate airflow patterns inside a volume representative of the right nasal passage of an anonymous adult male human. Volumetric flow rates were varied from 2 to 7 L/min corresponding to low physical activity (e.g., sitting or sleeping). Streamlines injected from several points on the nostril surface shown in Figure 2 exhibit laminar flow patterns throughout the nasal cavity. No major recirculation was observed, contrary to Swift and Proctor (1977), Schreck et al. (1993), and Kelly et al. (2000), and in agreement with Hahn et al. (1993), Keyhani et al. (1995), and Subramanian et al. (1998). As noted by the other authors, variations in anatomy will dictate different flow patterns. It should also be noted that the flow rates examined here are at the lower end of the other published studies.

Another method for observing vortices that may be too small for observation with streamlines is to measure the vorticity. Vorticity is, notionally, a measure of the circulation in a fluid flow about an infinitesimal point and is defined, mathematically, as the curl of the fluid velocity:

$$\zeta = \nabla \times \mathbf{u} \qquad [5]$$

While it is observed that the flow in the human nasal cavity exhibits laminar behavior, small local recirculation regions may be present in key areas. Figure 3 shows contours of vorticity perpendicular to coronal planes in the volume. The peak occurs posterior to the nasal valves, precisely where recirculation was observed by Swift and Proctor (1977), Schreck et al. (1993), and Kelly et al. (2000).

Volumetric airflow rates in various regions are estimated for a mean inlet flow rate of 5 L/min. and the results are shown in Figure 4. These estimates do agree with the published studies of Swift and Proctor (1977), Hahn et al. (1993) Schreck et al. (1993), and Kelly et al. (2000) in that the majority of the airflow passes through the inferior portion of the nasal cavity, and only a small fraction pass through the superior parts of the passage, in particular the olfactory region.

Particle Transport and Deposition

Several trials were run to examine the effects of particle size (diameter and density), breathing rate, and orientation of gravity on deposition efficiency. The diameter was varied from 1 μm to 10 μm in 1-μm increments, while the densities examined were 1, 2, and 3 g/cm^3 for a total of 30 particles' sizes. Mean inlet airflow rates of 2, 3, 4, 5, 6, and 7 L/min were investigated. The direction of the gravitational acceleration was set to the three orthogonal global axes and their respective complements. For each

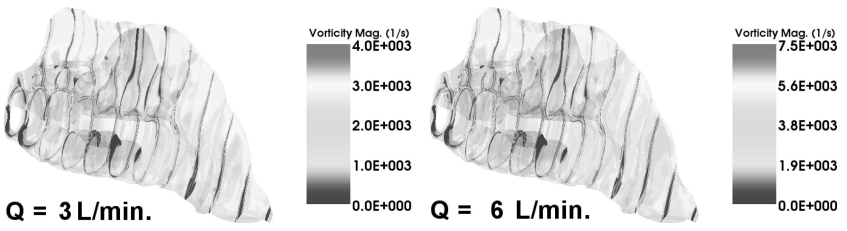

FIG. 3. Contours of vorticity perpendicular to coronal planes throughout the cavity for mean inlet flow rates of 3 and 6 L/min.

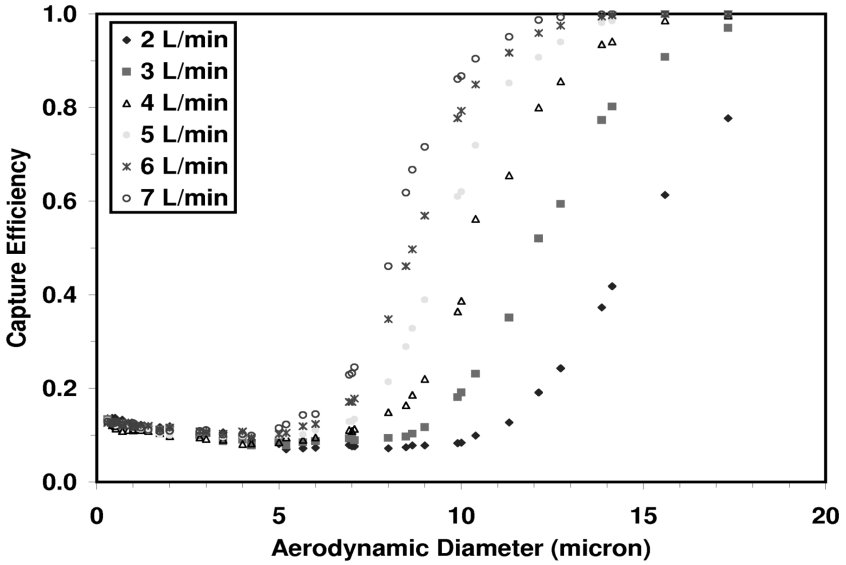

FIG. 5. Nasal cavity deposition efficiency as a function of aerodynamic diameter.

trial a single particle was released from the center of each computational cell on the inlet (nostril) surface, resulting in 1732 particles per trial. Each particle was tracked individually and due to the dilute concentrations one-way coupling was assumed. Sample planes were established at the entrance to the nasal valves, main airway, and nasopharynx. These sample planes counted the number of particles entering each region without perturbing their paths. Regional deposition fractions could be simply calculated by subtracting the number of particles entering the adjacent posterior region from the number entering the region of interest. The overall deposition efficiency is the sum of all regional deposition fractions.

Figure 5 shows nasal cavity deposition efficiency as a function of aerodynamic diameter for different flow rates. As expected, larger particles more readily impact the nasal surfaces, increasing the deposition efficiency of the cavity. Also obvious from Figure 5 is that breathing rate plays an important roll on deposition efficiency.

Figure 6 shows the use of impaction parameter ($\mathrm{IP} = d_{\mathrm{ac}}^2 Q$) to collapse all data from Figure 5 onto a single curve. Particles with higher IP have a higher deposition rate and particles with lower IP escape into the nasopharynx. Good agreement is seen between the present simulations and the available experimental data. Some slight deviations can be seen; particularly for low

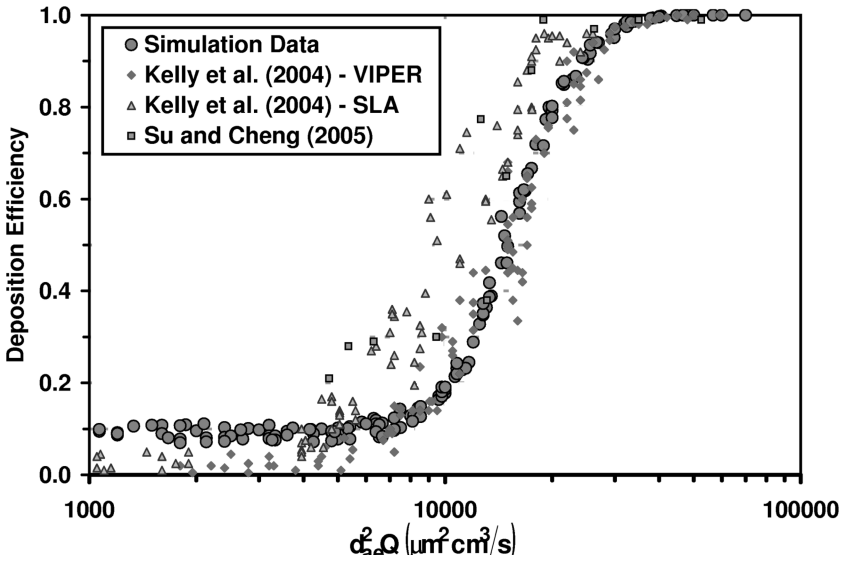

FIG. 6. Nasal cavity deposition efficiency as a function of impaction parameter.

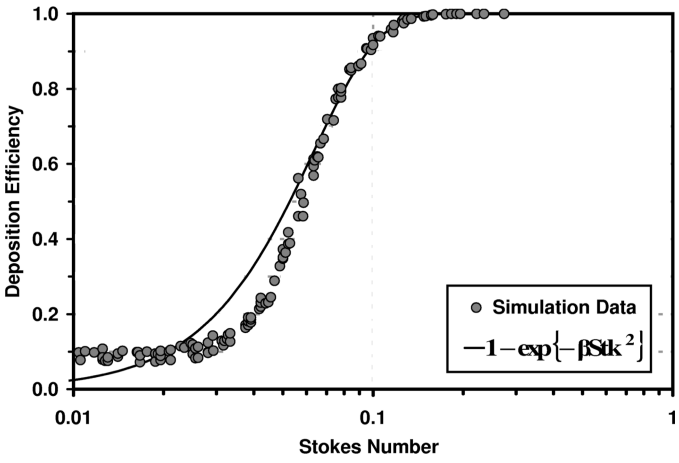

FIG. 7. Nasal cavity deposition efficiency as a function of Stokes number.

IP our simulations predict 4% to 5% greater deposition than the experimental data, and for mid-range IP the experiments show a more rapid increase in deposition efficiency than the present simulations. These differences can be most likely attributed to the large effects minor differences in anatomy can have on inertial deposition as explained by Kelly et al. (2004).

Introducing a suitable anatomical length scale, IP can be non-dimensionalized in the Stokes number (Stk) to account for subject-to-subject variability (Swift, 1991; Cheng, 2003). The Stokes number is defined as

$$\mathrm{Stk} = \frac{\sqrt{\pi}S}{18\nu A_C} IP \qquad [6]$$

Here A_C is the minimum cross-sectional area (79.9 mm^2 for the present model) of the cavity occurring in the nasal valve and S is the solid-to-gas density ratio. Unfortunately, A_C is unknown for the published experimental data presented in Figure 6; therefore, in Figure 7 only the present simulation results are shown.

An empirical expression for the deposition efficiency was developed to fit the present simulated data. This expression incorporates the effects of particle diameter and density, breathing rate, and anatomy of the subject through the appropriate length scale. That is,

$$E_\mathrm{d} = 1 - \exp[-ß(\mathrm{Stk})^2] \qquad [7]$$

Here the constant β in Eq. (7) is found to be 250.

Therapeutic aerosols provide a minimally invasive means for delivering relief to a patient. However, their effectiveness is highly dependent on where they deposit in the cavity. Figure 8 shows regional deposition fractions, as well as final fate destinations, for three representative Stokes number particles. Many of the smaller particles navigate through and escape with a small percentage depositing evenly throughout the cavity, while larger particles preferentially deposit in the anterior third of the cavity. This is believed to be because the anterior face of the turbinates jutting into the flow provides an ample surface for impaction and the fluid flow is transitioning from a high velocity/low cross section to a low velocity/high cross section.

The earth's gravitational field applies a force on a mass perpendicular to the earth's surface. A person could conceivably put him- or herself in various positions to change the direction in which this force acts on his or her head. This head orientation could be manipulated to enhance dosimetry during pharmaceutical delivery. While examining the entire infinite range of possible head orientations is impossible, there are three orthogonal directions along a global axis each with a complement. These six directions are shown on Figure 9. Each head orientation provides

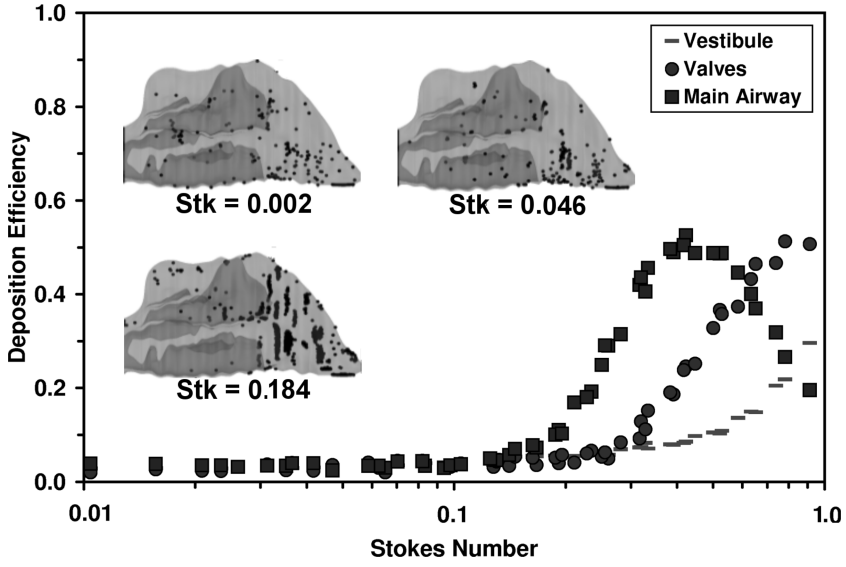

FIG. 8. Regional deposition efficiency as a function of stokes number with representative final fate destinations of three representative stokes number particles.

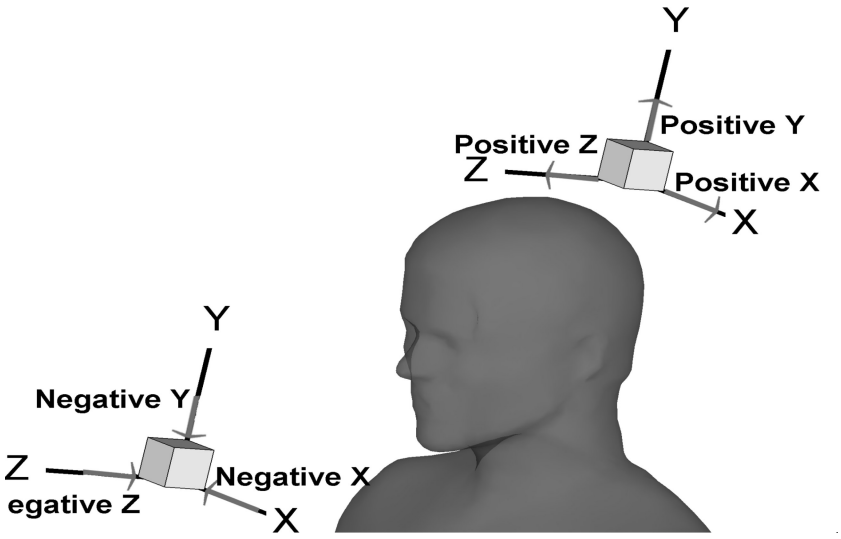

FIG. 9. Three orthogonal head orientations and their respective complements; *y* region for six different head orientations.

a unique direction for the terminal velocity vector. The terminal velocity is given as

$$u_t = g\,\tau \qquad [8]$$

For the size of particles and flow rates being considered, the terminal velocity is very small. However, for particles in the near-wall regions this added velocity, if in the direction of the wall, contributes to the deposition rate. On the contrary, an opposing direction of gravity will hinder the deposition rate. Figure 10 shows deposition efficiency as a function of Stokes number for all six head orientations shown in Figure 9, in addition to the case where gravity is absent. Little variation is seen between

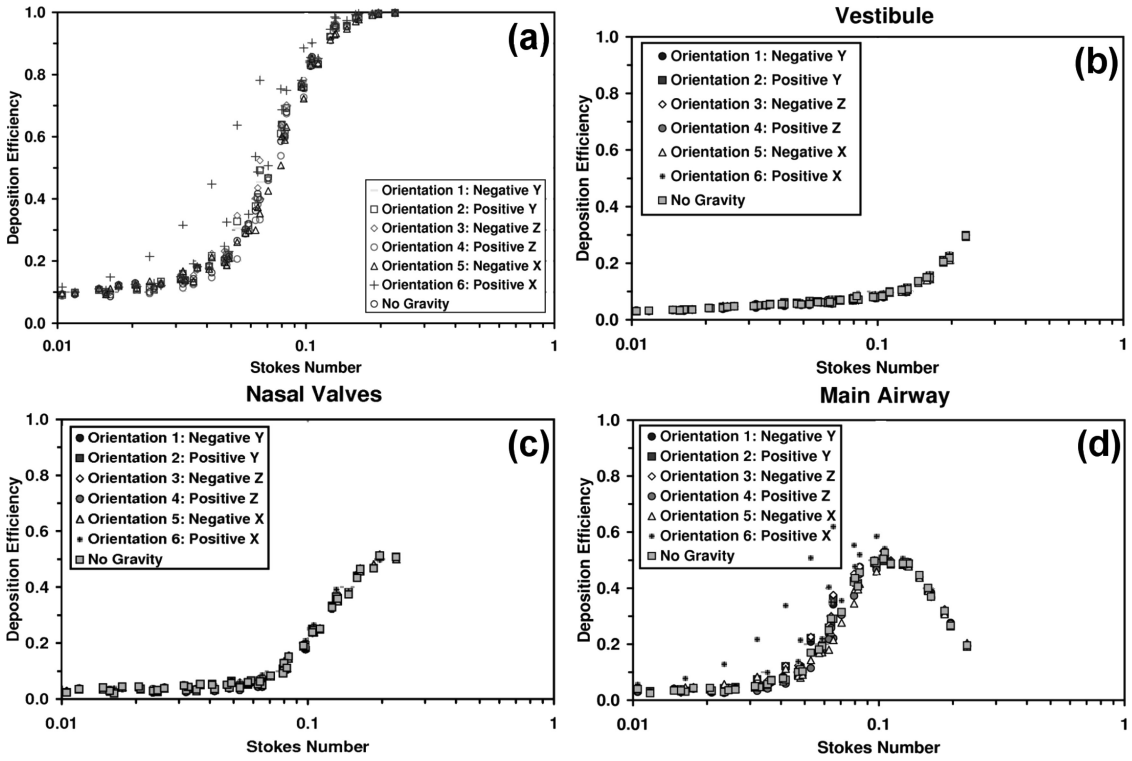

FIG. 10. Deposition efficiency as a function of Stokes number for six different head orientations in the (a) entire cavity, (b) vestibule, (c) valves, and (d) main airway region.

orientations except when gravity is aligned in the positive x-direction (laterally outward from the septum).

CONCLUSIONS

Airflow simulations and Lagrangian particle tracking of inertial particles have been carried out for a human nasal cavity anatomy reconstructed from MRI scans of an anonymous, adult, male, human subject. The airflow was taken to be steady, laminar, and inspiratory. A dilute, uniform concentration of particles was released at the nostril and tracked individually with a one-way coupling approach. A number of conclusions can be drawn from this study and are listed here:

- For low breathing rates laminar flow is an appropriate assumption.
- A peak in vorticity posterior to the nasal valves is present. This may lead to recirculation for higher flow rates.
- The inferior portions of the nasal cavity are where a majority of the inspired air travels.
- Impaction is the dominant deposition mechanism for particles greater than 1 μm in the human nasal cavity.
- Both impaction parameter and Stokes number collapse all deposition data onto a single curve.
- Smaller particles mostly escape into the nasopharynx, with a small percentage depositing evenly throughout the cavity
- Larger particles deposit with greater frequency and preferential deposition moves anterior with increasing Stokes number.
- Head orientation has small noticeable effects on regional or overall deposition.
- The proposed empirical expression, $E_d = 1 - \exp[-ß(\mathrm{Stk})^2]$, for the deposition efficiency agrees with the simulation data and includes the effect of particle size, particle density, breathing rate, and the subject's anatomy.

REFERENCES

Cheng, Y. S. 2003. Aerosol deposition in the extrathoracic region. *Aerosol Sci. Technol.* 37:659–671.

Cheng, Y. S., Holmes, T. D., Gao, J., Guilmette, R. A., Li, S., Surakitbanharn, Y., and Rowlings, C. 2001. Characterization of nasal spray pumps and deposition pattern in a replica of the human nasal airway. *J. Aerosol Med.* 14(2):267–280.

Cheng, Y.S., Yeh, H. C., Guilmette, R. A., Simpson, S. Q., Cheng, K. H., and Swift, D. L. 2006. Nasal deposition of ultrafine particles in human volunteers and its relationship to airway geometry. *Aerosol Sci. Technol.* 25:274–291.

Churchill, S. E., Shackelford, L. L., Georgi, J. N., and Black, M. T. 2004. Morphological variation and airflow dynamics in the human nose. *Am. J. Hum. Biol.* 16(6):625–638.

Dai, Y. T., Juang, Y. J., Wu, Y. Y., Breysse, P. N., and Hsu, D. J. 2006. In vivo measurements of inhalability of ultralarge aerosol particles in calm air by humans. *J. Aerosol Sci.* 37:967–973.

Fluent User's Manual. 2007. Version 6.3.26. Lebanon, NH: Fluent, Inc.

Hahn, I., Scherer, P. W., and Mozell, M. M. 1993. Velocity profiles measured for airflow through a large-scale model of the human nasal cavity, *J. Appl. Physiol.* 75:2273–2287.

Hinds, W. C. 1982. *Aerosol technology: Properties, behavior, and measurement of airborne particles*. New York: John Wiley and Sons.

Janssens, H. M., De Jongste, J. C., Fokkens, W. J., Robben, S. G. F., Wouters, K., and Tiddens, H. A. W. M. 2001. The Sophia Anatomical Infant Nose Throat (SAINT) model: A valuable tool to study aerosol deposition in infants. *J. Aerosol Med.* 14(4):433–441.

Kelly, J. T., Asgharian, B., Kimbell, J. S., and Wong, B. A. 2004 Particle deposition in human nasal airway replicas manufactured by different methods. Part I: Inertial regime particles. *Aerosol Sci. Technol.* 38:1063–1071.

Kelly, J. T., Prasad, A. K., and Wexler, A. S. 2000. Detailed flow patterns in the nasal cavity. *J. Appl. Physiol.* 89:323–337.

Keyhani, K., Scherer, P. W., and Mozell, M. M. 1995. Numerical simulation of airflow in the human nasal cavity. *J. Biomech. Eng.* 117:429–441.

Kim, S. K., and Chung, S. K. 2004. An investigation on airflow in disordered nasal cavity and its corrected models by tomographic PIV. *Meas. Sci. Technol.* 15:1090–1096.

Liu, Y., Matida, E. A., Gu, J., and Johnson, M. R. 2007. Numerical simulations of aerosol deposition in a 3-D human nasal cavity using RANS, RANS/EIM, and LES. *J. Aerosol Sci.* 38:693–700.

Martonen, T. B., and Zhang, Z. 1992. Comments on recent data for particle deposition in human nasal passages. *J. Aerosol. Sci.* 23(6):667–674.

Newman, S. P., Steed, K. P., Hooper, G., and Brickwell, J. 1995. Scintographic assessment of the oropharyngeal and nasal depositions of fusafungine from a pressurized inhaler and from a novel pump spray device. *J. Pharm. Pharmacol.* 47:818–821.

Schreck, S., Sullivan, K. J., Ho, C. M., and Chang H. K. 1993. Correlations between flow resistance and geometry in a model of the human nose. *J. Appl. Physiol.* 75:1767–1775.

Shi, H., Kleinstreuer, C., and Zhang, Z. 2007. Modeling of inertial particle transport and deposition in human nasal cavities with wall roughness. *J. Aerosol Sci.* 38:398–409.

Su, W. C., and Cheng Y. S. 2005. Deposition of fiber in the human nasal airway.*Aerosol Sci. Technol.* 39:888–901.

Subramanian, R. P., Richardson, R. B., Morgan, K. T., Kimbell, J. S., and Guilmette, R. A. 1998. Computational fluid dynamics simulations of inspiratory airflow in the human nose and nasopharynx, *Inhal. Toxicol.* 10:91–120.

Swift, D. L. 1991. Inspiratory inertial deposition of aerosols inhuman airway replicate casts: implication for the proposed NCRP lung model. *Radiat. Prot. Dosim.* 38:29–34.

Swift, D. L., and Proctor, D. F. 1977. Access of air to the respiratory tract. In *Respiratory Defense mechanisms: Part I,* eds. J. D. Brian, D. F. Proctor, and L. M. Reid, pp. 63–93. New York: Marcel Dekker.

Thorsson, L., Newman, S. P.,Weisz, A., Trofast, E., and Mor'en, F. 1993. Nasal distribution of budesonide inhaled via a powder inhaler. *Rhinology* 31:7–10.

Zamankhan, P., Ahmadi, G., Wang, Z., Hopke, P. K., Cheng, Y. S., Su, W. C., and Leonard, D. 2006. Airflow and deposition of nanoparticles in a human nasal cavity. *Aerosol. Sci. Technol.* 40:463–476.

Zwartz, G. J., and Guilmette, R. A. 2001. Effect of flow rate on particle deposition in a replica of a human nasal airway, *Inhal. Toxicol.* 13:109–127.